Journal: *Applied and Environmental Microbiology*

Section: Physiology

Metabolic Flux Hierarchy Prioritizes the Entner-Doudoroff Pathway for Carbohydrate Co-Utilization in *Pseudomonas protegens* Pf-5

Authors: Rebecca A. Wilkes[a], Caroll M. Mendonca[a], and Ludmilla Aristilde[a,#]

Affiliation: [a]Department of Biological and Environmental Engineering, College of Agriculture and Life Sciences, Cornell University, Ithaca, NY 14853, USA

[#]Corresponding author:

214 Riley-Robb Hall, Cornell University, Ithaca, NY 14850

Phone: (607) 255-6845. Fax: (607) 255-4449. E-mail: ludmilla@cornell.edu

Running head: Carbohydrate Metabolism in *Pseudomonas protegens* Pf-5

Keywords: *Pseudomonas*; co-utilization; metabolic flux analysis; hexose sugar; metabolomics

ABSTRACT. The genetic characterization of *Pseudomonas protegens* Pf-5 was recently completed. However, the inferred metabolic network structure has not yet been evaluated experimentally. Here we employed ^{13}C-tracers and quantitative flux analysis to investigate the intracellular network for carbohydrate metabolism. Similar to other *Pseudomonas* species, *P. protegens* Pf-5 relied primarily on the Entner-Doudoroff (ED) pathway to connect initial glucose catabolism to downstream metabolic pathways. Flux quantitation determined that, in lieu of the direct phosphorylation of glucose by glucose kinase, phosphorylation of oxidized products of glucose (gluconate and 2-ketogluconate) towards the ED pathway accounted for over 90% of

consumed glucose and greater than 35% of consumed glucose was secreted as gluconate and 2-ketogluconate. Consistent with the lack of annotated pathways for the initial catabolism of pentoses and galactose in *P. protegens* Pf-5, only glucose was assimilated into intracellular metabolites in the presence of xylose, arabinose, or galactose. However, when glucose was fed simultaneously with fructose or mannose, co-uptake of the hexoses was evident but glucose was preferred over fructose (3 to 1) and over mannose (4 to 1). Despite gene annotation of mannose catabolism toward fructose 6-phosphate, metabolite labeling patterns revealed that mannose-derived carbons specifically entered central carbon metabolism via fructose-1,6-bisphosphate, similarly to fructose catabolism. Remarkably, carbons from mannose and fructose were found to cycle backward through the upper Emden-Meyerhof-Parnas pathway to feed into the ED pathway. Therefore, the operational metabolic network for processing carbohydrates in *P. protegens* Pf-5 prioritizes flux through the ED pathway to channel carbons to downstream metabolic pathways.

IMPORTANCE. Species of the *Pseudomonas* genus thrive in various nutritional environments and have strong biocatalytic potential due to their diverse metabolic capabilities. Carbohydrate substrates are ubiquitous both in environmental matrices and in feedstocks for engineered bioconversion. Here we investigated the metabolic network for carbohydrate metabolism in *P. protegens* Pf-5. Metabolic flux quantitation revealed the relative involvement of different catabolic routes in channeling carbohydrate carbons through the network. We also uncovered that mannose catabolism was similar to fructose catabolism, despite the gene annotation of two different pathways in the genome. Elucidation of the constitutive metabolic network in *P. protegens* is important for understanding its innate carbohydrate processing, thus laying the foundation for targeting metabolic engineering of this untapped *Pseudomonas* species.

INTRODUCTION

Species of the genus *Pseudomonas,* which are ubiquitous in the environment, are metabolically diverse and often used for industrial bioproduction (1). Elucidating the native network of carbon fluxes through metabolic pathways is critical to the engineering of these bacterial species to optimize their use in agriculture, industry, and medicine. Gaining importance in bioremediation, *P. protegens* Pf-5 was identified to produce enzymes that degrade polyurethane, a plastic polymer (2). Furthermore, *P. protegens* Pf-5 is also known to synthesize and release several antimicrobials and exoenzymes that are toxic to plant pathogens (3–6). Recently, *P. protegens* Pf-5 was characterized and annotated at the genomic level (7). However, the metabolic network of *P. protegens* Pf-5 has only been inferred from genome annotation and has not yet been investigated experimentally.

Given the importance and ubiquity of carbohydrate-containing feedstocks, we seek to unravel the metabolic network structure for carbohydrate metabolism in *P. protegens* Pf-5 by combining ^{13}C-assisted cellular carbon mapping with ^{13}C metabolic flux analysis (MFA). Previous studies on other *Pseudomonas* species (i.e. *P. putida*, *P. fluorescens*) have focused on elucidating metabolic fluxes during growth on glucose, a prototypical carbohydrate substrate (8–11). In a similar fashion, we also studied here the innate carbohydrate metabolism in *P. protegens* Pf-5 during feeding on glucose alone. However, carbon feedstocks are typically composed of other carbohydrates in addition to glucose. Therefore, we also investigated carbon assimilation and fluxes when the *P. protegens* Pf-5 cells were fed on mixtures of glucose with other hexoses (mannose, fructose, and galactose) or pentoses (xylose and arabinose).

Previous reports showed that *P. protegens* strains were able to grow on glucose, mannose, or fructose as a single carbon source, but not on galactose, xylose, or arabinose (6). In the

genome of *P. protegens* Pf-5, the genes for the following transporters were encoded: a phosphoenolpyruvate (PEP):sugar phosphotransferase system (PTS) for fructose uptake (and possibly for mannose uptake) and ATP-binding cassette (ABC) transporters for glucose, mannose, galactose, and xylose (Fig. 1; Table S1) (7). Characteristically in *Pseudomonas* species, glucose metabolism involves a peripheral pathway in the periplasm wherein glucose dehydrogenase converts glucose to gluconate and gluconate 2-dehydrogenase converts gluconate to 2-ketogluconate (Fig. 1) (8). Fluxes through these oxidation reactions were found to maximize growth on glucose (8). After active transport into the cytoplasm, the oxidized products of glucose are phosphorylated to 6-phosphogluconate (6P-gluconate) and subsequently routed to the Entner-Doudoroff (ED) pathway or the pentose phosphate (PP) pathway (Fig. 1) (8, 10, 11). Previous studies with other *Pseudomonas* species have also determined that the forward Embden-Meyerhof-Parnas (EMP) pathway is not possible due to the absence of 6-phosphofructokinase to convert fructose 6-phosphate (F6P) to fructose 1,6-bisphosphate (FBP) (Fig. 1) (1, 7, 10). Therefore, to route glucose-derived carbons eventually downstream towards biosynthetic pathways and the tricarboxylic acid (TCA) cycle, the ED pathway is required wherein 6P-gluconate is cleaved to produce pyruvate and glyceraldehyde 3-phosphate (GAP) (Fig. 1). The gene that encodes 6-phosphofructokinase is also absent in *P. protegens* Pf-5 (7), thus the ED pathway is assumed to be the required route for glucose metabolism in *P. protegens* Pf-5. However, the extent to which the peripheral pathway of glucose oxidation contributes to initial glucose catabolism compared to direct glucose phosphorylation in *P. protegens* Pf-5 remains to be determined.

In contrast to glucose, fructose is transported through the PTS, which uses the phosphate group from PEP to phosphorylate fructose to fructose-1-phosphate (F1P) followed by a subsequent phosphorylation step by 1-phosphofructokinase to convert F1P to FBP (Fig. 1) (9,

12, 13). Previous studies on other *Pseudomonas* species (*P. fluorescens, P. putida, P. aeruginosa, P. stutzeri,* and *P. acidovorans*) reported that fructose-derived carbons were cycled back via a reverse flux through upper EMP pathway (FBP up to G6P) to be connected to the ED pathway (12, 14–16). However, according to the genome of *P. protegens* Pf-5, FBP could also be subjected to the last step of the EMP pathway wherein FBP can be lysed directly to two triose-phosphates, GAP and dihydroxyacetone-3-phosphate (DHAP) (Fig. 1) (7). Whether the preferential route for fructose assimilation during simultaneous feeding on glucose is via the lower EMP pathway or through the reverse cycling of carbons from FBP to ED pathway remains to be determined. The catabolic routing of FBP has important energetic implications for *P. protegens* Pf-5. Compared to the direct lysis through the forward EMP pathway, the combination of reverse flux through upper EMP pathway with the ED pathway maintains the same quantity of reduced equivalents (i.e., NAD(P)H) but half the ATP yield.

With respect to initial mannose catabolism, a previous study with *P. aeruginosa* proposed two possible routes, which involve either mannose isomerization to fructose followed by subsequent phosphorylation to FBP or direct phosphorylation of mannose to mannose 6-phosphate (M6P) prior to isomerization to F6P (17, 18). Relevant to the first route, an intracellular mannose isomerase (EC 5.3.1.7) was reported in *P. cepacia* and *P. saccharophila* (19, 20), but the gene for this enzyme was not annotated in the *P. protegens* Pf-5 genome (7). On the other hand, albeit not yet confirmed by metabolic studies, the genes for the relevant enzymes in the second catabolic route, i.e. the conversion of mannose to F6P, were annotated in the *P. protegens* Pf-5 genome (Fig. 1).

The presence of the annotated genes for transketolase and transaldolase enzymes implied a fully functional PP pathway in *P. protegens* Pf-5 (7). Both oxidative and non-oxidative routes of the PP pathway are important to channel carbohydrate-derived metabolite precursors to the

121 biosynthesis of ribonucleotides and aromatic amino acids. Regarding xylose catabolism, despite
122 the annotation of a ribose transporter that could be used as a possible xylose transporter, the
123 genes encoding the enzymes (xylose isomerase and xylulose kinase) responsible for introducing
124 xylose into the PP pathway were not present in *P. protegens* Pf-5 (Fig. 1) (7). Moreover, the
125 collective enzymes needed for the alternative route for xylose through the Weimberg pathway,
126 which incorporates xylose through xylonate into α-ketoglutarate, were not all present in the
127 genome of *P. protegens* Pf-5 (7). Regarding arabinose catabolism, there was no annotated
128 pathway for the assimilation of arabinose in *P. protegens* Pf-5 (Fig. 1) (7). Despite the lack of the
129 genes for xylose catabolism, a recent study reported extracellular xylose depletion by *P.*
130 *protegens* Pf-5 during growth on a mixture of carbohydrates (21). Whether arabinose or xylose
131 is incorporated into cellular metabolism, specifically the PP pathway, in the presence of another
132 carbohydrate remains to be determined.

133 Here we applied liquid chromatography (LC) with high-resolution mass spectrometry
134 (HRMS) to perform a ^{13}C-assisted metabolomics investigation during growth of *P. protegens* Pf-
135 5 on glucose alone or simultaneously with fructose, mannose, galactose, xylose, or arabinose.
136 We provide the first quantitative evaluation of the hypothetical metabolic network of *P.*
137 *protegens* Pf-5 deduced from its genome-level characterization. First, we employed carbon
138 mapping to identify the specific pathways that channel glucose-derived carbons throughout
139 cellular metabolism. Second, we performed quantitative analysis to determine energetic yields
140 from the cellular metabolism in *P. protegens* Pf-5. Third, we determined which carbohydrates
141 can be co-assimilated with glucose in *P. protegens* Pf-5 and subsequently quantified the
142 metabolic fluxes when co-utilization occurred. Our findings provide new metabolic insights,
143 which both resolve discrepant metabolic predictions from genome annotation and quantify
144 fluxes in the metabolic network structure for carbohydrate processing in *P. protegens* Pf-5.

RESULTS

Physiological Parameters of *P. protegens* Pf-5 Grown on Carbohydrate Mixtures. We investigated the growth phenotype of *P. protegens* during feeding on different hexose combinations. Our growth rates were in close agreement with reported values for glucose-grown *P. putida* (0.56 ± 0.02 h^{-1}) and *P. fluorescens* (0.49 ± 0.03 h^{-1}) (8, 22). At a total carbon equivalence of 100 mM C, the growth rate of cells fed on glucose alone (0.56 ± 0.09 h^{-1}) was similar to the growth rate of cells fed on a 1:1 mixture of glucose and fructose (0.52 ± 0.06 h^{-1}) or glucose and mannose (0.50 ± 0.04 h^{-1}) (Fig. 2A; Fig. S1; Table S2). We also found that the growth rate remained relatively unchanged when the cells were grown on 50 mM C glucose alone (0.47 ± 0.02 h^{-1}) (Fig. 2A). Therefore, *P. protegens* would not be subjected to carbon limitation during growth on carbohydrate mixtures if either fructose or mannose was not assimilated from the mixture with glucose (Fig. 2A).

We monitored substrate consumption by *P. protegens* Pf-5 cells by tracking the depletion of the carbohydrates from the extracellular medium (Fig. 2B; Table S2). The glucose-grown cells depleted glucose completely over a 10 h period (Fig. 2B). Over the same period of time, the cells grown on the mixture of glucose and mannose depleted both substrates completely but cells grown on the mixture of glucose and fructose depleted glucose completely and fructose partially (Fig. 2B). We also observed that, during growth of *P. protegens* Pf-5 on the glucose:mannose mixture, fructose appeared in the extracellular medium about 1 h after mannose consumption started (Fig. 2A). The appearance of extracellular fructose implied the presence of mannose isomerase, which was responsible for converting mannose to fructose in other *Pseudomonas* species (19,20) (Fig. 2B). During growth on both hexose mixtures, glucose was consumed faster and depleted by 6 h of growth, at which time about 30% of the fructose

was consumed but only 10% of mannose was taken up by the cells (Fig 2B). Quantification of the consumption rates during exponential growth determined that fructose consisted 22% of the total carbon uptake and mannose consisted of 20% of total carbon uptake (Table S2). Thus, during hexose co-utilization under both of our experimental conditions, glucose acts as the major carbon source for cellular metabolism.

We also monitored the extracellular overflow of metabolic products, a phenomenon that is widely reported in *Pseudomonas* species (8, 11, 23). Both oxidized products of glucose (i.e., gluconate and 2-ketogluconate) and the organic acid pyruvate were found in appreciable levels (above 0.001 mM) in the extracellular medium (Fig. 2C). Secretions of gluconate and 2-ketogluconate were also reported with *P. putida* (8, 11) and *P. fluorescens* (23); pyruvate secretion was also reported in *P. fluorescens* (23). The levels of these secreted metabolites were dependent on substrate composition in the growth medium of *P. protegens*. The highest secretions of gluconate and 2-ketogluconate (greater than 2 mM) were measured in the medium when cells were grown on glucose alone or glucose with fructose. By contrast, during growth on the glucose:mannose mixture, the highest secretion of gluconate and 2-ketogluconate decreased substantially, by ~40% and ~85%, respectively (Fig. 2C; Table S2). Compared to gluconate and 2-ketogluconate, pyruvate was secreted in smaller amounts (µM range), with the highest secretion (0.13 ± 0.08 mM) obtained when cells were grown on glucose alone (Fig. 2C; Table S2).

Metabolic Pathways and Fluxes in Glucose-Fed Cells. Isotopic enrichment with [1,2-$^{13}C_2$]-glucose was used to determine the metabolic network structure through initial glucose catabolism, the EMP pathway, the ED pathway, the PP pathway, and the TCA cycle (Fig. 3). At two timepoints during exponential growth, we obtained similar metabolite ^{13}C-labeling

193 patterns, which confirmed pseudo-steady state isotopic enrichment (Fig. 3). To elucidate fluxes
194 through 48 reactions in the metabolic pathway, we combined the metabolite labeling data with
195 substrate consumption rates (accounting for excretion of gluconate and 2-ketogluconate) and
196 biomass growth rates (Fig. 4A; Fig. S2; Table S3; Table S4). Adjusting for the carbon loss through
197 metabolite secretions, about 64% of the glucose consumed from the extracellular medium was
198 available for intracellular catabolism in *P. protegens* Pf-5. Very close alignment between the
199 MFA-estimated labeling patterns and those determined experimentally reflected the quality of
200 the optimization procedure for the model cellular fluxes (Fig. S3).
201 *Involvement of glucose oxidation and the ED pathway*. Glucose catabolism can be initiated
202 via three different routes: direct phosphorylation to G6P, oxidation to gluconate in the
203 periplasm before phosphorylation to 6P-gluconate, or additional periplasmic oxidation of
204 gluconate to 2-ketogluconate before phosphorylation to 6P-gluconate (Fig. 1). Doubly ^{13}C-
205 labeled 6P-gluconate (86-89%) and doubly ^{13}C-labeled G6P (~63%) were both consistent with
206 the assimilation of [1,2-$^{13}C_2$]-glucose (Fig. 3A). In accordance with the ED pathway wherein the
207 first three carbons of 6P-gluconate become the doubly ^{13}C-labeled pyruvate and the last three
208 nonlabeled carbons become GAP, pyruvate was 50-53% doubly ^{13}C-labeled and DHAP (an
209 isomer of GAP) was over 95% nonlabeled (Fig. 3A). The 37-38% nonlabeled fraction of pyruvate
210 was indicative of the nonlabeled fractions of precursor metabolites downstream of GAP (Fig.
211 3A). In the absence of the 6-phosphofructokinase enzyme in *P. protegens* Pf-5 and thus the lack
212 of the traditional forward EMP pathway (7), the nonlabeled GAP and DHAP combined to
213 produce the highly nonlabeled FBP (85-87%), which then cycled backward through upper EMP
214 to result in the 67-70% nonlabeled F6P and 31% nonlabeled G6P (Fig. 3A). The MFA quantified
215 the relative contribution of the three assimilation routes for the glucose carbons in *P. protegens*
216 Pf-5 (Fig 4A). Only ~5% of the glucose uptake was directly converted to G6P in the cytosol,

whereas up to 95.2% of glucose was oxidized to gluconate accompanied by another flux (12.7%) toward 2-ketogluconate (Fig. 4A). Following the phosphorylation of the oxidized products of glucose to 6P-gluconate, our MFA determined that the flux through the ED pathway was 67.2% of the glucose uptake rate in *P. protegens* Pf-5 (Fig. 4A).

Oxidative versus non-oxidative PP pathway. Following a decarboxylation reaction through the oxidative PP pathway, doubly ^{13}C-labeled 6P-gluconate would become singly ^{13}C-labeled Ru5P, which would introduce singly ^{13}C-labeled fractions into metabolites in the PP pathway (Fig. 3B). Thus, singly ^{13}C-labeled fractions of xylulose 5-phosphate (Xu5P) (21-25%), ribose 5-phosphate (R5P) (22-25%), and sedoheptulose 7-phosphate (S7P) (20-23%) were due to flux through the oxidative PP pathway (Fig. 3B). However, by involving nonlabeled metabolites from downstream of the ED pathway, the non-oxidative PP pathway introduced relatively higher nonlabeled fractions of Xu5P (64-67%), R5P (65-69%), and S7P (62-69%) (Fig. 3B). Accordingly, the MFA determined an oxidative flux to the PP pathway (about 0.5%), which was a tenth of the non-oxidative PP pathway fluxes (5.1%) from ketolase and transaldolase reactions (Fig. 3B and 4A). As a precursor to both the oxidative PP pathway and the ED pathway, 6P-gluconate represents an important branch point in metabolism. Therefore, the low contribution of 6P-gluconate to the oxidative PP pathway necessitated a reverse flux from downstream ED pathway to the upper EMP pathway (i.e. gluconeogenesis) to channel glucose-derived carbons towards the PP pathway in support of biomass growth (Fig. 4A).

Downstream metabolic pathways. The ^{13}C-labeling patterns of TCA cycle intermediates were consistent with the established route of carbon flow through this pathway (Fig. 3C). The decarboxylation of pyruvate generated nonlabeled and singly ^{13}C-labeled acetyl moieties in acetyl-CoA, which were subsequently incorporated into the TCA cycle by combining with oxaloacetate (OAA) (nonlabeled, singly, doubly, and minorly triply ^{13}C-labeled) to produce

241 citrate (nonlabeled, singly, doubly, triply, and minorly quadruply ^{13}C-labeled) (Fig 3C). The two
242 sequential decarboxylation reactions in the TCA cycle led to the disappearance of the quadruply
243 ^{13}C-labeled fraction in citrate and, thereafter, the triply ^{13}C-labeled fraction in α-ketoglutarate
244 (Fig. 3C). The resulting succinate labeling pattern (nonlabeled, singly, and doubly ^{13}C-labeled)
245 led to a similar labeling scheme through fumarate, malate, and OAA (Fig. 3C). The MFA
246 obtained a substantial flux (above 70% of the glucose uptake) through the TCA cycle from OAA
247 around to malate (Fig. 4A).

248 Anaplerotic reactions contributed to the triply ^{13}C-labeled OAA (Fig. 3C). The
249 aforementioned decarboxylation reactions in the TCA cycle contributed to the ^{13}C-labeled
250 carbon dioxide (CO_2) pool, which was calculated to be about 37-39% of the total dissolved CO_2
251 (Fig. 3; Fig. S4). The carboxylation of doubly ^{13}C-labeled pyruvate or doubly ^{13}C-labeled PEP with
252 ^{13}C-labeled CO_2 would generate triply ^{13}C-labeled OAA (Fig. 3C). Notably, singly ^{13}C-labeled OAA
253 can be formed from carboxylation reactions of nonlabeled pyruvate or PEP with singly ^{13}C-
254 labeled CO_2 (Fig. 3C). The singly ^{13}C-labeled OAA can also be formed from singly ^{13}C-labeled
255 malate though the traditional TCA pathway utilizing malate dehydrogenase (Fig. 3C). The
256 relative contributions of the different precursors to OAA (i.e., pyruvate/PEP versus malate) in *P.*
257 *protegens* Pf-5 was resolved with the MFA, which demonstrated a substantially higher
258 fractional flux of pyruvate to OAA (70%) than the flux of malate to OAA through malate
259 dehydrogenase (7.7%) (Fig. 4A). This low flux through malate dehydrogenase was accompanied
260 by a high flux for the direct conversion of malate to pyruvate (63.4%), thus highlighting a very
261 active pyruvate shunt in *P. protegens* Pf-5 (Fig. 4A). The ^{13}C-labeling patterns of TCA cycle
262 metabolites implied an inactive glyoxylate shunt, which bypasses the decarboxylation reactions
263 in the canonical TCA cycle to produce malate and succinate from citrate (Fig. S5). Specifically,

264 there was a lack of triply ^{13}C-labeled succinate which would be produced from triply and
265 quadruply ^{13}C-labeled citrate through the glyoxylate shunt (Fig. S5).
266 *Energetics of glucose catabolism*. We compared the energetic yields [reduced ubiquinone
267 (UQH_2), NAD(P)H, and ATP] from central carbon metabolism between our MFA-based cellular
268 fluxes in *P. protegens* Pf-5 and those previously reported for *P. putida* KT2440, a well-studied
269 biocatalyst candidate (10) (Fig. 4B). Compared to *P. putida* KT2440 (10), there was a slightly
270 higher flux (about 5% higher) from glucose to gluconate in *P. protegens* Pf-5 but the flux from
271 malate to OAA was lower (by about 25%) in *P. protegens* Pf-5. Accordingly, there was a higher
272 yield of UQH_2 from initial glucose catabolism in *P. protegens* Pf-5 but a higher UQH_2 yield from
273 the TCA cycle in *P. putida* KT2440 (Fig. 4B). Regarding the yield of NAD(P)H, there was a higher
274 contribution from the TCA cycle (by about 3%) and from the oxidative PP pathway (by about
275 60%) in *P. putida* KT2440 than in *P. protegens* Pf-5 but the contribution of the anaplerotic
276 reaction from malate to pyruvate was lower (by about 81%) in *P. putida* KT2440 than in *P.*
277 *protegens* Pf-5 (Fig. 4B). With respect to ATP production by substrate-level phosphorylation, *P.*
278 *protegens* Pf-5 produced less (by about 3 mmol ATP/g_{CDW}) than *P. putida* KT2440 due to the
279 relatively lower fluxes in the downstream ED pathway of *P. protegens* (10) (Fig. 4). However,
280 the net ATP yield was similar because *P. protegens* Pf-5 consumed less ATP than *P. putida*
281 KT2440 in initial glucose catabolism due to the higher flux for the glucose oxidation to
282 gluconate and 2-ketogluconate and accounting for the subsequent carbon loss through
283 secretions of these oxidized products in *P. protegens* Pf-5 (10) (Fig. 4). In sum, despite the
284 different contributions of the relevant metabolic pathways, the combination of these
285 contributions led to nearly equivalent net energetic yields in *P. protegens* Pf-5 and *P. putida*
286 KT2440 (Fig. 4B).
287

Hierarchy of Glucose Metabolism in the Presence of Other Carbohydrates.

Proof of concept with ^{13}C-labeled glucose and unlabeled glucose. Before determining the relative incorporation of [U-$^{13}C_6$]-glucose in the presence of a nonlabeled carbohydrate (xylose, arabinose, galactose, fructose, or mannose), we first conducted proof-of-concept experiments with the cells grown on [U-$^{13}C_6$]-glucose alone or in a 1:1 mixture with unlabeled glucose (Fig. 5; Fig. 6) (24). By comparative analysis with the metabolite labeling patterns in the latter two conditions, we seek to determine the relative incorporation of other unlabeled carbohydrates in the presence of [U-$^{13}C_6$]-glucose (Fig. 5; Fig. 6).

Glucose with xylose, arabinose, or galactose. While galactose, xylose, and arabinose are reported to not be metabolized as single substrates in *P. protegens* Pf-5 (6), whether they are metabolized in the presence of glucose needed to be evaluated. During growth on ^{13}C-labeled glucose and galactose, the labeling patterns of metabolites in the EMP and ED pathways (F6P, FBP, DHAP) were identical to the metabolite labeling during feeding on glucose alone, thus indicating the lack of galactose catabolism in the presence of glucose (Fig. 5A). During simultaneous feeding on ^{13}C-labeled glucose and a pentose substrate (xylose or arabinose), the labeling patterns of metabolites in the PP pathway (Xu5P, R5P, S7P) also indicated the lack of pentose assimilation (Fig. 5B). Furthermore, there was no indication of xylose incorporation into α-ketoglutarate, consistent with the lack of the Weimberg pathway (Fig. S6). Therefore, our data from ^{13}C enrichment studies ascertained the absence of carbon assimilation from galactose, xylose, or arabinose in the presence of glucose (Fig. 5).

Glucose with Fructose. Following simultaneous feeding on [U-$^{13}C_6$]-glucose and unlabeled fructose, a persistence of nonlabeled fractions in the intracellular metabolites was consistent with both uptake and assimilation of fructose in the presence of glucose (Fig. 6). However, the differential abundance of the nonlabeled fractions indicated a bottleneck in fructose

assimilation, which may explain the slower rate of fructose depletion than glucose depletion from the extracellular medium (Fig. 2B; Fig. 6). Consistent with fructose incorporation through F1P into FBP, the highest fraction of nonlabeled carbons was seen in FBP (59-62%); both F6P and DHAP had lower nonlabeled fractions (25-30% and 17%, respectively) (Fig. 6). The lower fraction of nonlabeled carbons in DHAP than in F6P implied that the fructose-derived carbons were preferentially routed through a backward flux through upper EMP pathway towards the ED pathway (Fig. 6). The labeling of G6P reflected the nonlabeled and partially ^{13}C-labeled fractions from F6P, consistent with this backward flux (Fig. 6). Therefore, in lieu of the forward EMP pathway, our data stresses the importance of the ED pathway in the co-processing of fructose with glucose.

The labeling patterns of metabolites in the PP pathway also showed that the contribution of the fructose-derived carbons in this pathway was preferentially through the non-oxidative route (Fig. 6). A transketolase reaction in the non-oxidative PP pathway combines the first two carbons of F6P with GAP to produce Xu5P. Both Xu5P and R5P have significant fractions of triply ^{13}C-labeled carbons (38-44%), in accordance with the combination of nonlabeled F6P with triply ^{13}C-labeled GAP following growth on ^{13}C-labeled glucose with unlabeled fructose (Fig. 6). Due to the low fraction of nonlabeled GAP (as determined from DHAP labeling), there was a lack of appreciable fraction of doubly ^{13}C-labeled R5P and Xu5P, which was evident in cells grown on [U-$^{13}C_6$]-glucose with unlabeled glucose (Fig. 6).

Glucose with mannose. In contrast to the metabolite labeling during growth on [U-$^{13}C_6$]-glucose with unlabeled fructose, the metabolite labeling patterns following feeding on the [U-$^{13}C_6$]-glucose with unlabeled mannose showed delayed assimilation of mannose into intracellular metabolism during exponential cell growth (Fig. 6). This was evident by the substantial increase in the nonlabeled fraction of FBP at the two timepoints, from 12% at an

optical density at 600 nm (OD_{600}) of ~0.5 to 52% at OD_{600} of ~1.0 (Fig. 6). This time-dependent labeling data agreed with the fact that extracellular mannose started to decrease significantly after 6 h of growth, following the depletion of glucose (Fig. 2B).

A higher nonlabeled fraction of FBP than of F6P implied that incorporation of mannose-derived carbons into FBP by way of fructose was preferred in *P. protegens* Pf-5 (Fig. 6). In agreement with this catabolic route for mannose, there was a larger pool of FBP than F6P when cells were grown on the glucose:mannose mixture relative to the glucose only condition (Fig. S7). This large FBP pool was also seen in the glucose:fructose condition relative to the glucose only condition (Fig. S7). During feeding on ^{13}C-glucose with unlabeled mannose, the nonlabeled fraction of DHAP (18%) was lower than F6P (28%) and G6P (26%) (Fig. 6). Therefore, these labeling data collectively indicated the cycling of nonlabeled mannose carbons backward through the upper EMP pathway towards the ED pathway, similar to the intracellular metabolism of fructose (Fig. 6).

Cellular Carbon Fluxes during Co-utilization of Glucose and Fructose. Quantitative MFA was used to assess differences in the metabolic fluxes during growth on glucose alone versus growth on glucose with fructose (Fig. 7; Table S4; Table S5). Our MFA focused on the pathways surrounding the incorporation points of carbohydrates: initial glucose catabolism, the EMP pathway, PP pathway, and the ED pathway (Fig. 7). Each MFA made use of the labeling data collected at OD_{600} of 0.5 during early exponential phase before extracellular glucose is depleted and was constrained by the consumption rate of each carbohydrate, biomass effluxes, and metabolite secretions (Fig. 7; Fig. S2; Table S5; Table S6). Upon optimization of the estimated metabolic fluxes, the model-estimated ^{13}C-labeling patterns agreed well with the experimentally determined ^{13}C-labeling patterns for each condition (Fig. S8; Fig. S9).

Despite the genome-encoded capabilities in *P. protegens* Pf-5 to involve the splitting of FBP to DHAP and GAP (Paulsen et al., 2005), the MFA revealed that the net flux was instead the aldolase reaction that combines DHAP and GAP to generate FBP (Fig. 7). Due to the additional incorporation of fructose-derived carbons through the flux from FBP to 6P-gluconate, there were higher fluxes from FBP to F6P (3-fold increase), F6P to G6P (3.6-fold increase), and G6P to 6P-gluconate (2.3-fold increase) in cells grown on the glucose:fructose mixture compared to glucose alone (Fig. 7). Similar to metabolism of glucose alone, there was a significant flux of the glucose uptake channeled through glucose oxidation to gluconate (88%) followed by the ED pathway (95%) during the metabolism of both glucose and fructose (Fig. 7). Consistent with the increased carbon flux towards 6P-gluconate, there were a 4.3-fold increase in the flux toward the oxidative PP pathway (i.e. from 6P-gluconate to Ru5P) and a 19% increase in the ED pathway (i.e., from 6-gluconate to GAP and pyruvate) (Fig. 7).

Kinetic Isotope Analysis during Co-utilization of Glucose and Mannose. Due to the lack of isotopic pseudo-steady state during simultaneous growth on glucose and mannose, ^{13}C-MFA could not be conducted. To capture the assimilation route for mannose, we obtained measurements of metabolic isotopic fractions during six timepoints during exponential growth of ^{13}C-labeled glucose and unlabeled mannose (Fig. 8). Specifically, we examined the labeling patterns of gluconate, 6P-gluconate, G6P, F6P, FBP, and DHAP (Fig. 8). Across all timepoints, gluconate labeling was consistently ~100% fully ^{13}C-labeled, indicating that gluconate was exclusively the oxidized product of the ^{13}C-labeled glucose (Fig 8). However, the labeling of the other five metabolites had nonlabeled fractions derived from the assimilation of unlabeled mannose (Fig. 8). The labeling of 6P-gluconate exhibited the slowest kinetic incorporation of nonlabeled fractions (Fig. 8). The appearance of nonlabeled pool of 6P-gluconate (starting at

384 ~4%) occurred at the fifth measurement timepoint at an OD_{600} of 0.94 (Fig. 8). By contrast, FBP
385 exhibited the fastest incorporation of nonlabeled fraction that occurred at an OD_{600} of 0.2 (Fig.
386 8). Compared to the labeling kinetics of FBP, there was a delay in the incorporation of
387 nonlabeled carbons in F6P and G6P, which started to occur an OD_{600} of 0.6, and DHAP, which
388 steadily increased after an OD_{600} 0f 0.8 (Fig. 8). Statistical analysis (Mixed Effect Model; $F_{3, 57}$ =
389 12.973; $p < 0.0001$) confirmed that the significant effect of OD_{600} on the incorporation of
390 mannose-derived nonlabeled carbons was dependent on the metabolite (Fig. 8). These kinetics
391 data collectively demonstrated that, instead of being channeled directly from FBP to GAP and
392 DHAP, mannose carbons were incorporated at FBP and cycled up through F6P and G6P to the
393 ED pathway to generate subsequently GAP and DHAP (Fig. 8). Thus, the catabolic route for
394 mannose was similar to what was determined for fructose catabolism.
395

396 **DISCUSSION**

397 The metabolic networks and fluxes of several *Pseudomonas* species, including *P. putida, P.*
398 *fluorescens,* and *P. aeruginosa*, have been previously described (8–11, 22, 25). Here we present
399 the first metabolic flux analysis of the recently characterized *P. protegens* Pf-5, a common plant
400 commensal bacterium known to secrete specialized metabolites important for the biocontrol of
401 fungi and bacteria pathogenic to plants (4, 6). Metabolic flux quantitation determined that
402 initial glucose catabolism in *P. protegens* Pf-5 was primarily through periplasmic oxidation to
403 gluconate with relatively minor influx of glucose through G6P (Fig. 4A). Up to 95% of consumed
404 glucose in *P. protegens* Pf-5 was channeled through the ED pathway, which was also reported in
405 *P. putida*, *P. fluorescens,* and *P. aeruginosa* (8, 11, 22, 25). Furthermore, the non-oxidative
406 route was more significant than the oxidative route in generating PP pathway intermediates in
407 *P. protegens* Pf-5, as previously reported for *P. putida* KT2440 (11) (Fig. 3B; Fig. 4A). The highly

active flux of pyruvate formation from malate in the *P. protegens* Pf-5 cells was also reported in *P. putida* and *P. fluorescens* (8, 10, 22). In sum, our results stressed that the metabolic network for glucose metabolism in *P. protegens* Pf-5 is consistent with the metabolic network of previously studied species of the *Pseudomonas* genus. Finally, through the contribution of different metabolic pathways, the total energetic yields of *P. protegens* Pf-5 were remarkably similar to *P. putida* KT2440, whose metabolism was been featured for its capability for fulfilling high demands of reducing power (10).

Root exudates and the breakdown of polysaccharides from plant biomass both provide various carbohydrates that stimulate growth of soil microorganisms, including *Pseudomonas* species (26). With respect to the catabolism of other carbohydrates besides glucose, we found that *P. protegens* Pf-5 did not metabolize the common hemicellulose monomers galactose, xylose, or arabinose in the presence of glucose but did utilize the carbon mixtures of glucose with fructose or mannose (Fig. 5; Fig. 6). In accordance with gene annotations, metabolite labeling data confirmed that fructose was incorporated into metabolism via FBP (Fig. 6). However, contrary to the possible route for mannose assimilation through F6P annotated in the *P. protegens* Pf-5 genome (7), the primary route of mannose assimilation in *P. protegens* Pf-5 was found to be also via FBP (Fig. 6). In addition, the appearance of fructose extracellularly during growth on mannose implied conversion of mannose to fructose prior to intracellular metabolism (Fig. 2B). Mannose conversion to fructose by a mannose isomerase has been reported previously in *P. cepacia, P. aeruginosa,* and *P. saccharophila* (17–20). Whether a non-specific isomerase exists in *P. protegens* remains to be determined.

The cyclic metabolism linking backward flux from FBP through the upper EMP towards the ED pathway produces equivalent NADPH, but less net ATP, compared to direct FBP conversion to GAP and DHAP. Interestingly, instead of this direct contribution to the lower EMP pathway,

carbons from assimilated fructose and mannose were routed through the cyclic connection between upper EMP pathway and the ED pathway during mixed-substrate utilization (Fig. 7; Fig. 8). Comparable MFA findings were reported for fructose-only catabolism in *P. putida* KT2440 and *P. fluorescens* SBW25 (14, 16). Therefore, *P. protegens* Pf-5 exhibits a strong reliance on the ED pathway for both fructose and mannose assimilation even in the presence of glucose.

Similar growth phenotypes during co-utilization of hexoses implied that, despite different carbohydrates in the growth medium at the same total carbon equivalence, *P. protegens* Pf-5 preserved a constant biomass maintenance (Fig. 2A). However, uptake of glucose was preferred over the uptake of fructose (3 to 1) or mannose (4 to 1) (Fig. 2; Table S2). The composition ratio of glucose to fructose in maize root exudates was found to be 2 to 1 (27). And, across soil horizons, the glucose:mannose ratio ranged approximately from 3:1 to 5:1 (28). Therefore, remarkably, the relative consumption rates of glucose versus fructose or mannose in *P. protegens* Pf-5 were in agreement with relative composition of these carbohydrates in environmentally-relevant conditions.

Related to the potential of *P. protegens* Pf-5 as a biocatalytic platform, the innate production and secretion of gluconate and 2-ketogluconate in *P. protegens* Pf-5 are additional attractive features. Oxidized sugars are important precursors to polymeric materials including polyesters. In fact, gluconate was identified as a top 30 value-added candidate for production of bio-inspired materials (29). Under our experimental conditions, the secretion rates of gluconate and 2-ketogluconate collectively accounted for about 35% of the glucose uptake in *P. protegens* during exponential growth whereas metabolite secretion of gluconate was reported to be less 10% of the glucose uptake in *P. putida* KT2440 (11) (Fig. 2C). While there were relatively similar secretions during growth on glucose alone or glucose and fructose, growth on glucose and

456 mannose resulted in a decrease in the total secretion (by about 3.5 mM) of gluconate and 2-
457 ketogluconate (Fig. 2C). After glucose was depleted, a decrease in the concentration of both
458 gluconate and 2-ketogluconate indicated that the cells can utilize these metabolites once their
459 favored carbon source is exhausted (Fig. 2B; Fig. 2C). This phenomenon would need to be
460 considered and manipulated to harvest these metabolite secretions in *P. protegens* Pf-5 as
461 valuable products. In light of the abundance of different types of carbohydrates in renewable
462 carbon feedstocks in natural environments and in use for engineered bioproduction (30), our
463 findings collectively provide important insights regarding the cellular metabolism underlying
464 carbohydrate co-utilization in *P. protegens* Pf-5 and related *Pseudomonas* species.
465
466 **MATERIALS AND METHODS**
467 **Materials.** The *P. protegens* Pf-5 cells were acquired from the American Type Culture Collection
468 (Manassas, VA). Unless noted otherwise, chemicals used in the growth media were obtained
469 from Sigma-Aldrich (St. Louis, MO), Cayman Chemical (Ann Arbor, MI), or Fisher Scientific
470 (Pittsburgh, PA). The ^{13}C -labeled glucose ([U-$^{13}C_6$]-glucose and [1,2-$^{13}C_6$]-glucose) were
471 purchased from Cambridge Isotopes (Tewskbury, MA) and Omicron Biochemicals (South Bend,
472 IN), respectively. All culture solutions were prepared with Millipore water (18.2 MΩ cm,
473 Millipore; Billerica, MA, USA) while resuspensions for LC-HRMS analysis were made with LC-MS
474 grade water. Solutions were sterilized by passing through a 0.22-µm nylon filters (Waters
475 Corporation, MA). An Agilent Cary UV-visible spectrophotometer (Santa Clara, CA) was used for
476 optical density readings at 600 nm. The LC-HRMS analysis was conducted on an ultra-high-
477 performance LC (Thermo scientific DionexUltiMate 3000) coupled to a high-
478 resolution/accurate-mass MS (Thermo Scientific Q Exactive quadrupole-Oribitrap hybrid MS)
479 with electrospray ionization.

Culturing conditions and growth measurements. Batch growth experiments (three to seven biological replicates) of *P. protegens* Pf-5 were conducted in an incubator (model I24; New Brunswick Scientific, Edison, NJ) maintained at 30°C and shaken at 220 rpm. Initial growth in nutrient-rich medium prior to growth in minimal-nutrient medium was conducted as previously described (11). Final growth experiments were conducted in 125-mL baffled flasks with a pH-adjusted (7.0) and filter-sterilized minimal-nutrient medium that contained major salts and essential trace metal nutrients as previously reported (31): 89.4 mM K_2HPO_4, 56.4 mM NaH_2PO_4, 0.81 mM $MgSO_4 \cdot 7H_2O$, 18.7 mM NH_4Cl, 8.6 mM NaCl, 34 µM $CaCl_2 \cdot 2 H_2O$, 30 µM $FeSO_4 \cdot 7 H_2O$, 0.86 µM $CuSO_4 \cdot 5 H_2O$, 1.9 µM H_3BO_3, 7.7 µM $ZnSO_4 \cdot 7 H_2O$, 0.75 µM $MnSO_4 \cdot 5 H_2O$, 0.26 µM $NiCl_2 \cdot 6 H_2O$, and 0.3 1µM $Na_2MoO_4 \cdot 5 H_2O$. The carbohydrate composition was 100 mM C total for glucose alone (equivalent to 16.7 mM or 3 g L^{-1} glucose) and for 1:1 glucose:xylose, glucose:arabinose, glucose:galactose, glucose:mannose, or glucose:fructose. For cellular isotopic enrichment, either [U-$^{13}C_6$]-glucose or [1,2-$^{13}C_6$]-glucose was used in glucose-only growth, but only [U-$^{13}C_6$]-glucose was used for mixtures in combination with an unlabeled second carbohydrate. Bacterial growth in the biological replicates was monitored as a function of time until late stationary phase using OD_{600} measurements (Fig. S1)—cell suspensions were diluted when the OD_{600} value was above 0.5 to get accurate reading. Cell dry weight in grams (g_{CDW}) was also determined throughout growth by lyophilizing the cell pellets as previously described (11).

Measurement of Carbohydrate Consumption. Independent ^{13}C-tracer experiments, as described in the next section, confirmed that extracellular depletion of the substrates correlated with substrate consumption. The extracellular depletion of each carbohydrate

504 substrate (three biological replicates) was determined throughout 24 h of cell growth. Culture
505 aliquots were pelleted by centrifugation and the supernatant was stored at -20 °C until further
506 analysis. Following previously reported LC methods for carbohydrate analysis (21), we applied
507 an analytical method using LC-HRMS for monitoring carbohydrate concentration in the
508 extracellular solution. Peak identification and quantification of carbohydrate concentrations
509 were conducted with ThermoScientific Xcalibur™ 3.0 Quan Browser.
510
511 **Metabolite Monitoring and Quantification.** *Extracellular Metabolites*. To determine metabolite
512 excretion rates, cell suspension samples (three biological replicates) were harvested
513 periodically throughout growth and pelleted with centrifugation before the supernatant was
514 removed and stored at -20 °C until LC-HRMS analysis. Dilutions of 1:10, 1:100, and 1:1000 were
515 conducted to account for the varying concentrations of each metabolite over time. For the LC,
516 an Acquity UPLC Waters 1.7 µm particle size column with dimensions of 2.1 x 100 mm was used
517 for all metabolomics samples (Milford, MA) with constant column temperature of 25°C. The
518 flow rate was kept constant at 0.180-mL min^{-1}. The mobile phase composition and LC protocol
519 were as previously described (31). The injection volume for each sample was 10-µL. The MS was
520 operated in full scan negative mode. Metabolite identification was based on accurate mass and
521 matches with standard retention time. Metabolite levels were quantified using
522 ThermoScientific Xcalibur™ 3.0 Quan Browser.
523 *Intracellular Metabolites.* Cells were separated by filtration and then lysed to extract
524 intracellular metabolites as described in Sasnow et al. (11). Metabolites in solution were
525 monitored by LC-HRMS and the ^{13}C labeling patterns were analyzed on the Metabolomic
526 Analysis and Visualization Engine (MAVEN) software (32, 33). Isotopologue data were obtained
527 for the following compounds: 6P-gluconate, G6P, F6P, FBP, DHAP, 3-phosphoglycerate, PEP,

528 pyruvate, Xu5P, R5P, S7P, aspartate, citrate, α-ketoglutarate, succinate, and malate. Aspartate
529 ^{13}C-labeling is used as a proxy for OAA ^{13}C-labeling by assuming equilibrium between the two
530 compounds (11). The labeling of dissolved CO_2 was estimated from the labeling patterns of
531 ornithine and citrulline (Fig. S2); ornithine incorporates one mole of dissolved CO_2 to become
532 citrulline. All the extracted isotopologues were corrected for natural abundance of ^{13}C. To verify
533 pseudo-steady state isotopic enrichment of the intracellular pools, metabolites were isolated
534 from cellular extracts obtained at two different timepoints during the exponential phase, at
535 OD_{600} values of ~0.5 and ~1.0 (11). To analyze mannose incorporation over time, cells were
536 extracted at six timepoints during exponential growth corresponding to OD_{600} values of ~0.2,
537 ~0.4, ~0.6, ~0.8, ~0.9, and ~1.3. A mixed effect model was conducted using R (34) and the
538 lmerTest package (35), which modeled the nonlabeled fraction (log transformed) by OD_{600},
539 metabolite, and their interaction with the random effect of biological replicate.
540
541 **Quantitative Metabolic Flux Modeling.** Quantitation of the metabolic fluxes was achieved for
542 cells grown on glucose alone and glucose with fructose. We employed the following
543 experimental data to constrain the metabolic flux analysis: substrate uptake rate, metabolite
544 excretions, growth rate, and cellular stoichiometry. Carbon effluxes from intermediates in
545 central metabolism towards biomass production were determined based on the growth rate for
546 each condition and the biomass composition of *P. putida* (nucleic acids, proteins, cell
547 membrane, and carbohydrate polymers) (36). An initial reaction network for the central carbon
548 metabolism of *P. protegens* PF-5 was constructed using predicted genome-scale metabolic
549 model (7), and gene annotation of metabolic enzymes reported on the KEGG database (37–39),
550 and MetaCyc (40). The metabolic reaction network was validated through ^{13}C-labeling of
551 intracellular metabolites. The following reactions were constrained in the forward direction:

552 gluconate → 6P-gluconate, 6P-gluconate → ribulose 5-phosphate, gluconate → 2-
553 ketogluconate, 2-ketogluconate → 6P-gluconate, glucose → G6P, FBP → F6P, malate →
554 pyruvate, pyruvate → OAA, and PEP → OAA. Optimized fluxes in the model metabolic network
555 reactions were determined by the 13CFLUX2 software package (http://www.13cflux.net) (41)
556 whereby quality of fit was optimized iteratively by comparing experimental ^{13}C-labeling data
557 and the *in silico*-estimated labeling data.
558
559 **SUPPLEMENTAL MATERIAL**
560 Supplemental material can be found in the online version of this article.
561
562 **ACKNOWLEDGEMENTS**
563 Graduate financial support for R.A.W and C.M.M. was provided in part by the College of
564 Agriculture and Life Sciences at Cornell University. We are grateful to Dr. Krista A. Barzen-
565 Hanson from the Aristilde Research Group at Cornell University (presently at Elmira College) for
566 her technical assistance in implementing the LC-MS protocol to analyze the carbohydrate
567 compounds in solution. We acknowledge Erika Mudrak at the Cornell Statistical Consulting Unit
568 for her assistance with implementing and interpreting the statistical analysis.
569
570 **REFERENCES**
571 1. Singh PB, Saini HS, Kahlon RS. 2016. *Pseudomonas*: The Versatile and Adaptive Metabolic
572 Network, p. 81–126. *In* Pseudomonas: Molecular and Applied Biology. Springer
573 International Publishing, Cham.
574 2. Hung C-S, Zingarelli S, Nadeau LJ, Biffinger JC, Drake CA, Crouch AL, Barlow DE, Russell JN,
575 Crookes-Goodson WJ. 2016. Carbon catabolite repression and Impranil polyurethane

degradation in *Pseudomonas protegens* strain Pf-5. Appl Environ Microbiol 82:6080–6090.

3. Loper JE, Gross H. 2007. Genomic analysis of antifungal metabolite production by *Pseudomonas fluorescens* Pf-5. Eur J Plant Pathol 119:265–278.

4. Loper JE, Kobayashi DY, Paulsen IT. 2007. The genomic sequence of *Pseudomonas fluorescens* Pf-5: insights into biological control 97.

5. Nowak-Thompson B, Gould J, Kraus J, Loper E. 1994. Production of 2,4-diacetylphloroglucinol by the biocontrol agent *Pseudomonas fluorescens* Pf-5. Can J Microbiol 40:1064–1066.

6. Ramette A, Frapolli M, Saux MF, Gruffaz C, Meyer J, Défago G, Sutra L, Moënne-loccoz Y. 2011. *Pseudomonas protegens* sp. nov., widespread plant-protecting bacteria producing the biocontrol compounds 2,4-diacetylphloroglucinol and pyoluteorin. Syst Appl Microbiol 34:180–188.

7. Paulsen IT, Press CM, Ravel J, Kobayashi DY, Myers GSA, Mavrodi D V, DeBoy RT, Seshadri R, Ren Q, Madupu R, Dodson RJ, Durkin AS, Brinkac LM, Daugherty SC, Sullivan SA, Rosovitz MJ, Gwinn ML, Zhou L, Schneider DJ, Cartinhour SW, Nelson WC, Weidman J, Watkins K, Tran K, Khouri H, Pierson EA, Pierson LS, Thomashow LS, Loper JE. 2005. Complete genome sequence of the plant commensal *Pseudomonas fluorescens* Pf-5. Nat Biotechnol 23:873–878.

8. Del Castillo T, Ramos JL, Rodríguez-Herva JJ, Fuhrer T, Sauer U, Duque E. 2007. Convergent peripheral pathways catalyze initial glucose catabolism in *Pseudomonas putida*: Genomic and flux analysis. J Bacteriol 189:5142–5152.

598 9. Chavarría M, Kleijn RJ, Sauer U, Pflüger-grau K, Lorenzo V De. 2012. Regulatory tasks of
599 the phosphoenolpyruvate-phosphotransferase system of *Pseudomonas putida* in central
600 carbon metabolism. MBio 3:1–9.
601 10. Nikel PI, Chavarría M, Fuhrer T, Sauer U, Lorenzo V De. 2015. *Pseudomonas putida*
602 KT2440 metabolizes glucose through a cycle formed by enzymes of the Entner-
603 Doudoroff, Embden-Meyerhof-Parnas, and Pentose Phosphate pathways 1–29.
604 11. Sasnow SS, Wei H, Aristilde L. 2016. Bypasses in intracellular glucose metabolism in iron-
605 limited *Pseudomonas putida*. Microbiologyopen 5:3–20.
606 12. Van Dijken JP, Quayle JR. 1977. Fructose metabolism in four *Pseudomonas* species. Arch
607 Microbiol 114:281–6.
608 13. Rojo F. 2010. Carbon catabolite repression in *Pseudomonas* : optimizing metabolic
609 versatility and interactions with the environment. FEMS Microbiol Rev 34:658–684.
610 14. Lien SK, Niedenführ S, Sletta H, Nöh K, Bruheim P. 2015. Fluxome study of Pseudomonas
611 fluorescens reveals major reorganisation of carbon flux through central metabolic
612 pathways in response to inactivation of the anti-sigma factor MucA. BMC Syst Biol 9:6.
613 15. Sawyer MH, Baumann P, Baumann L, Berman SM, Canovas JL, Berman RH. 1977.
614 Pathways of d-fructose catabolism in species of *Pseudomonas*. Arch Microbiol 112:49–
615 55.
616 16. Sudarsan S, Dethlefsen S, Blank LM, Siemann-Herzberg M, Schmid A. 2014. The
617 functional structure of central carbon metabolism in *Pseudomonas putida* KT2440. Appl
618 Environ Microbiol 80:5292–303.
619 17. Eagon RG, Williams AK. 1960. Enzymatic patterns of adaptation to fructose, glucose, and

mannose exhibited by *Pseudomonas aeruginosa*. J Bacteriol 79:90–94.

18. Hu X, Shi Y, Zhang P, Miao M, Zhang T, Jiang B. 2016. d -Mannose: Properties, production, and applications: An overview. Compr Rev Food Sci Food Saf 15:773–785.

19. Allenza P, Morrell MJ, Detroy RW. 1990. Conversion of mannose to fructose by immobilized mannose isomerase from *Pseudomonas cepacia*. Appl Biochem Biotechnol 24:171–182.

20. Palleroni NJ, Doudoroff M. 1956. Mannose isomerase of *Pseudomonas saccharophila*. J Biol Chem 218:535–548.

21. Barzen-Hanson KA, Wilkes RA, Aristilde L. 2018. Quantitation of environmentally relevant carbohydrate monomers and dimers by liquid chromatography coupled with high-resolution mass apectrometry. Carbohydr Res.

22. Fuhrer T, Fischer E, Sauer U. 2005. Experimental identification and quantification of glucose metabolism in seven bacterial species. J Bacteriol 187:1581–90.

23. Asai T, Aida K, Sugisaki Z, Yakeishi N. 1955. On a-ketoglutaratic acid fermentation. J Gen Appl Microbiol 1:308–346.

24. Aristilde L. 2017. Metabolite labelling reveals hierarchies in *Clostridium acetobutylicum* that selectively channel carbons from sugar mixtures towards biofuel precursors. Microb Biotechnol 10:162–174.

25. Berger A, Dohnt K, Tielen P, Jahn D, Becker J, Wittmann C. 2014. Robustness and plasticity of metabolic pathway flux among uropathogenic isolates of *Pseudomonas aeruginosa*. PLoS One 9:e88368.

26. Gunina A, Kuzyakov Y. 2015. Soil biology & biochemistry sugars in soil and sweets for

642 microorganisms : Review of origin, content, composition and fate. Soil Biol Biochem
643 90:87–100.
644 27. Hütsch BW, Augustin J, Merbach W. 2002. Plant rhizodeposition — an important source
645 for carbon turnover in soils. J Plant Nutr Soil Sci 165:397.
646 28. Benzing-Purdie L. 1980. Organic matter and carbohydrate distribution in an orthic humic
647 gleysol. Soil Biol Biochem 12:567–571.
648 29. Werpy T, Petersen G, Aden A, Bozell J, Holladay J, White J, Manheim A, Eliot D, Lasure L,
649 Jones S. 2004. Top value-added chemicals from biomass. volume 1-Results of screening
650 for potential candidates from sugars and synthesis gas. Washington DC.
651 30. Poblete-Castro I, Becker J, Dohnt K, dos Santos VM, Wittmann C. 2012. Industrial
652 biotechnology of *Pseudomonas putida* and related species. Appl Microbiol Biotechnol
653 93:2279–2290.
654 31. Aristilde L, Reed ML, Wilkes RA, Youngster T, Kukurugya MA, Katz V, Sasaki CRS. 2017.
655 Glyphosate-induced specific and widespread perturbations in the metabolome of soil
656 *Pseudomonas* species. Front Environ Sci 5:34.
657 32. Clasquin MF, Melamud E, Rabinowitz JD. 2012. LC-MS data processing with MAVEN: A
658 metabolomic analysis and visualization engine, p. Unit14.11. *In* Current Protocols in
659 Bioinformatics. John Wiley & Sons, Inc., Hoboken, NJ, USA.
660 33. Melamud E, Vastag L, Rabinowitz JD. 2010. Metabolomic analysis and visualization
661 engine for LC−MS data. Anal Chem 82:9818–9826.
662 34. R Core Team. 2016. R: A language and environment for statistical computing. R
663 Foundation for Statistical Computing, Vienna, Austria.

664 35. Kuznetsova A, Brockhoff P, Christensen R. 2017. lmerTest package: Tests in linear mixed
665 effects models. J Stat Softw 82:1–26.
666 36. van Duuren JB, Puchałka J, Mars AE, Bücker R, Eggink G, Wittmann C, dos Santos VA.
667 2013. Reconciling in vivo and in silico key biological parameters of *Pseudomonas putida*
668 KT2440 during growth on glucose under carbon-limited condition. BMC Biotechnol 13:93.
669 37. Kanehisa M, Sato Y, Kawashima M, Furumichi M, Tanabe M. 2016. KEGG as a reference
670 resource for gene and protein annotation. Nucleic Acids Res 44:D457–D462.
671 38. Kanehisa M, Goto S. 2000. KEGG: kyoto encyclopedia of genes and genomes. Nucleic
672 Acids Res 28:27–30.
673 39. Kanehisa M, Furumichi M, Tanabe M, Sato Y, Morishima K. 2017. KEGG: new perspectives
674 on genomes, pathways, diseases and drugs. Nucleic Acids Res 45:D353–D361.
675 40. Caspi R, Altman T, Dreher K, Fulcher CA, Subhraveti P, Keseler IM, Kothari A,
676 Krummenacker M, Latendresse M, Mueller LA, Ong Q, Paley S, Pujar A, Shearer AG,
677 Travers M, Weerasinghe D, Zhang P, Karp PD. 2012. The MetaCyc database of metabolic
678 pathways and enzymes and the BioCyc collection of pathway/genome databases. Nucleic
679 Acids Res 40:D742–D753.
680 41. Weitzel M, Nöh K, Dalman T, Niedenführ S, Stute B, Wiechert W. 2013. 13CFLUX2--high-
681 performance software suite for (13)C-metabolic flux analysis. Bioinformatics 29:143–5.
682

683 **FIGURES**

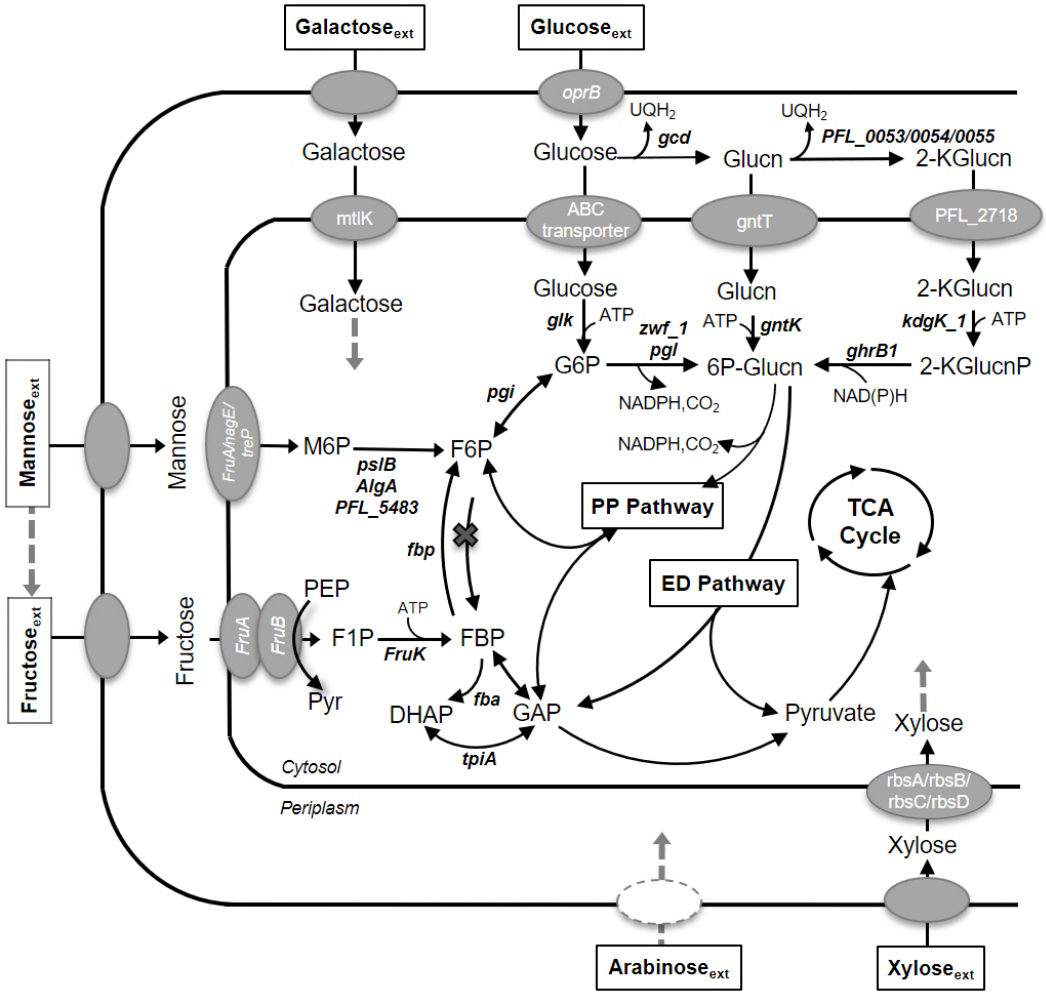

684

685 **FIG 1.** Putative genes involved in the uptake and initial catabolism of glucose, galactose,
686 mannose, fructose, xylose, and arabinose into central metabolism. The gene annotations for
687 pathways were collected from KEGG database (37–39) and MetaCyc database (40) for *P.*
688 *protegens* Pf-5. The corresponding gene loci for the genes in the figure are shown in Table S1.
689 The abbreviations are as follows: gluconate, Glucn; 2-ketogluconate, 2-KGlucn; 2-keto-6-
690 phosphogluconate, 2-KGlucnP; glucose 6-phosphate, G6P; 6-phosphogluconate, 6P-Glucn;
691 fructose 6-phosphate, F6P; fructose 1,6-bisphosphate, FBP; dihydroxyacetone-3-phosphate,
692 DHAP; glyceraldehyde 3-phosphate, GAP; fructose 1-phosphate, F1P; pyruvate, Pyr;
693 phosphoenolpyruvate, PEP.

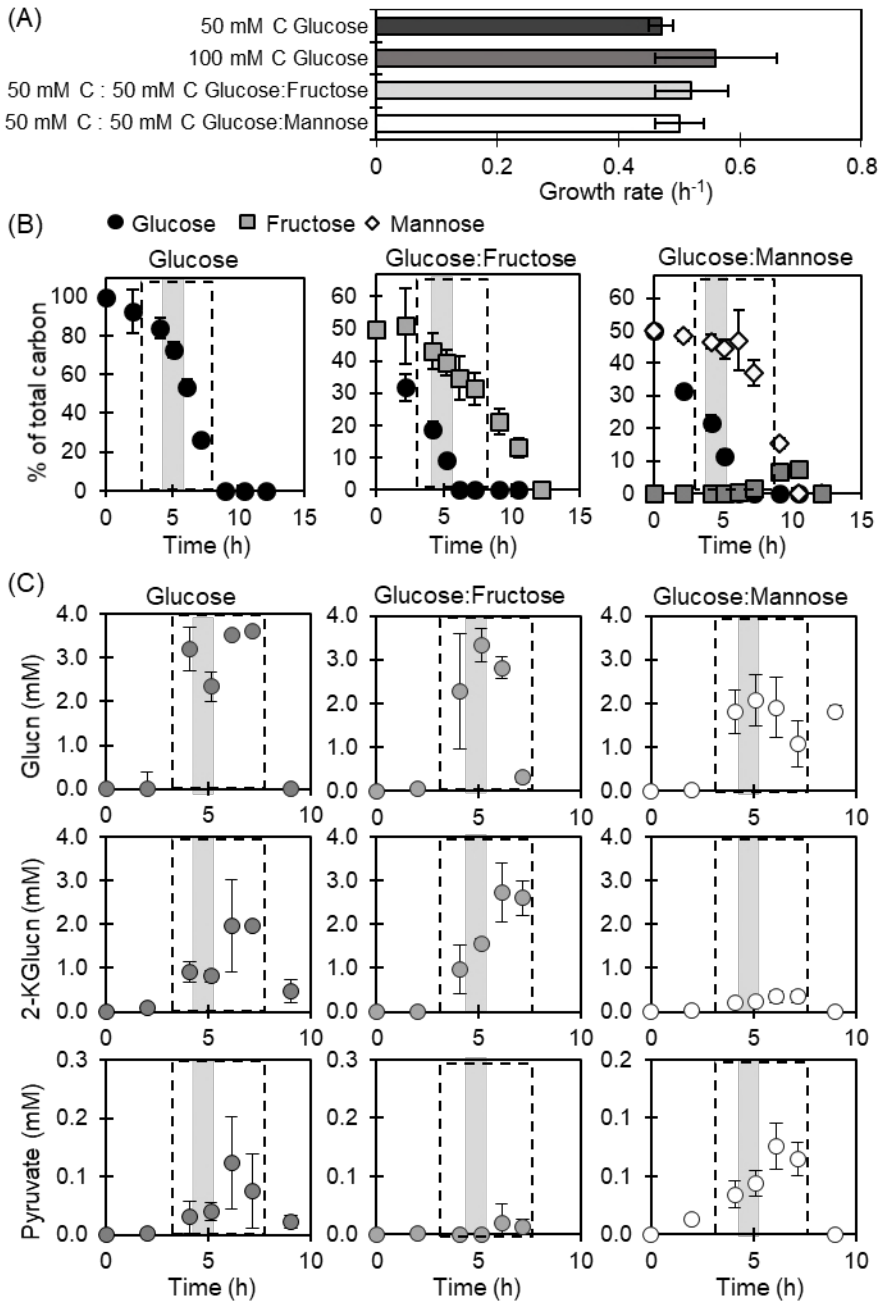

694 **FIG 2.** (A) Growth rate, (B) kinetic profile of carbohydrate depletion, and (C) kinetic profile of
695 metabolite secretions for cells fed glucose only or equimolar glucose:fructose or
696 glucose:mannose. Initial total carbohydrate concentration was 100 mM C (3 g L^{-1}). In B and C,
697 the data points within the dashed box were obtained during exponential growth; the shaded
698 area at an OD_{600} of 0.5 corresponds to the timepoint for the measured labeling data used for
699 the MFA. Data are shown as means ± standard deviation from biological replicates (*n* = 3).
700

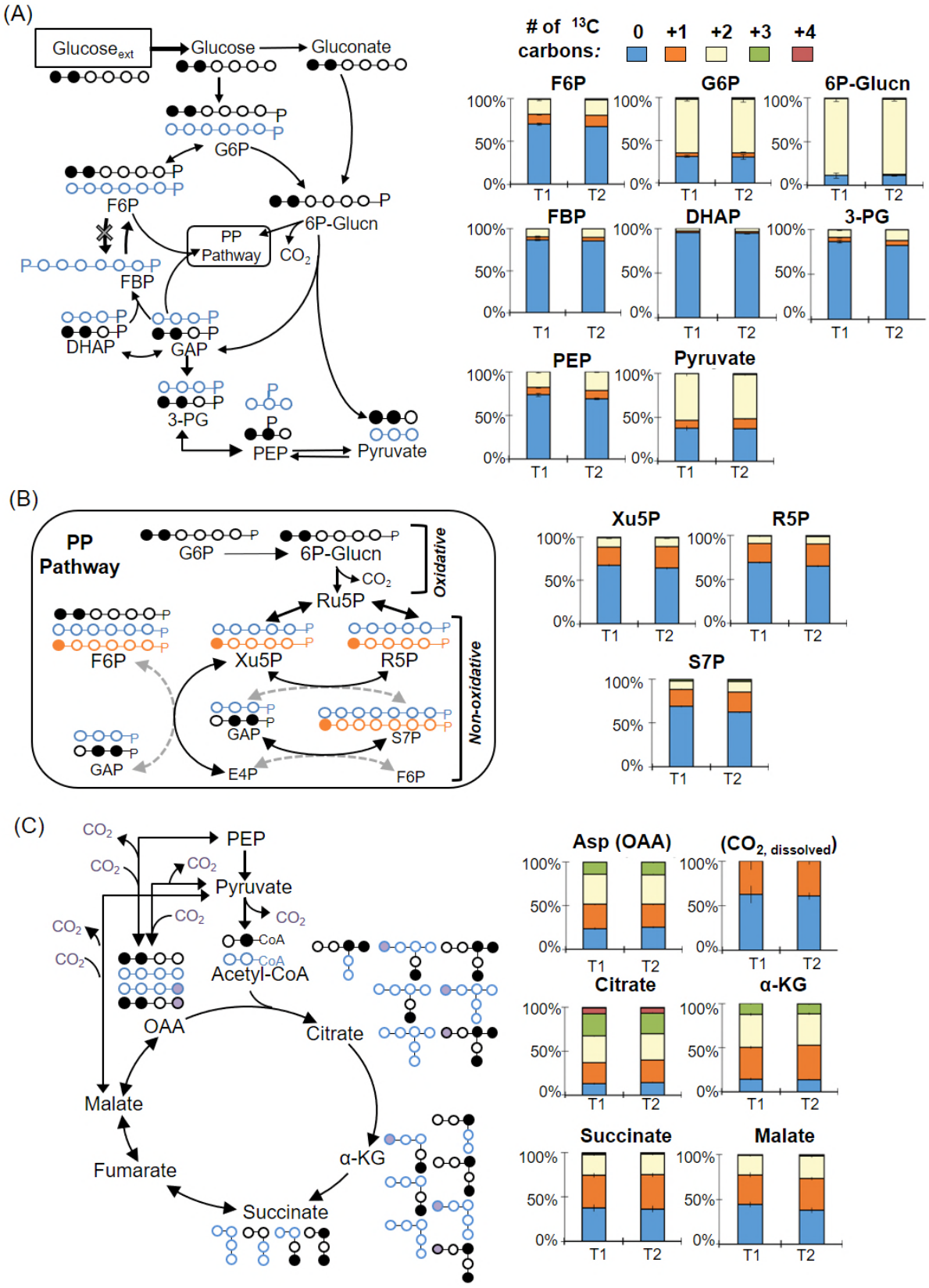

701

FIG 3. Long-term isotopic enrichment with [1,2-$^{13}C_2$]-glucose for carbon mapping of the metabolic network structure in *P. protegens* Pf-5. Carbon mapping is illustrated on the left and the metabolite labeling data are provided on the right for the following: (A) Initial glucose catabolism, Embden-Meyerhof-Parnas (EMP) pathway, and the Entner-Doudoroff (ED) pathway; (B) Oxidative and non-oxidative routes of the pentose-phosphate (PP) pathway; (C) the tricarboxylic acid (TCA) cycle. The dashed arrows describe minor formation routes of the metabolites. In the carbon mapping, blue represents the fate of structures derived from the ED and reverse-EMP pathways and orange represents the fate of structures derived from the oxidative PP pathway. Labeling patterns: nonlabeled (light blue), singly labeled (orange), doubly labeled, (cream), triply labeled (green), and quadruply labeled (red). Labeling data (average ± standard deviation) were from three independent biological replicates. The abbreviations are as follows: gluconate, Glucn; 2-ketogluconate, 2-KGlucn; glucose 6-phosphate, G6P; 6-phosphogluconate, 6P-Glucn; fructose 6-phosphate, F6P; fructose 1,6-bisphosphate, FBP; dihydroxyacetone-3-phosphate, DHAP; glyceraldehyde 3-phosphate, GAP; phosphoenolpyruvate, PEP; 3-phosphoglycerate, 3PG; xylulose 5-phosphate, Xu5P; ribose 5-phosphate, R5P; sedoheptulose 7-phosphate, S7P; oxaloacetate, OAA; aspartate, Asp; α-ketogluconate, α-KG.

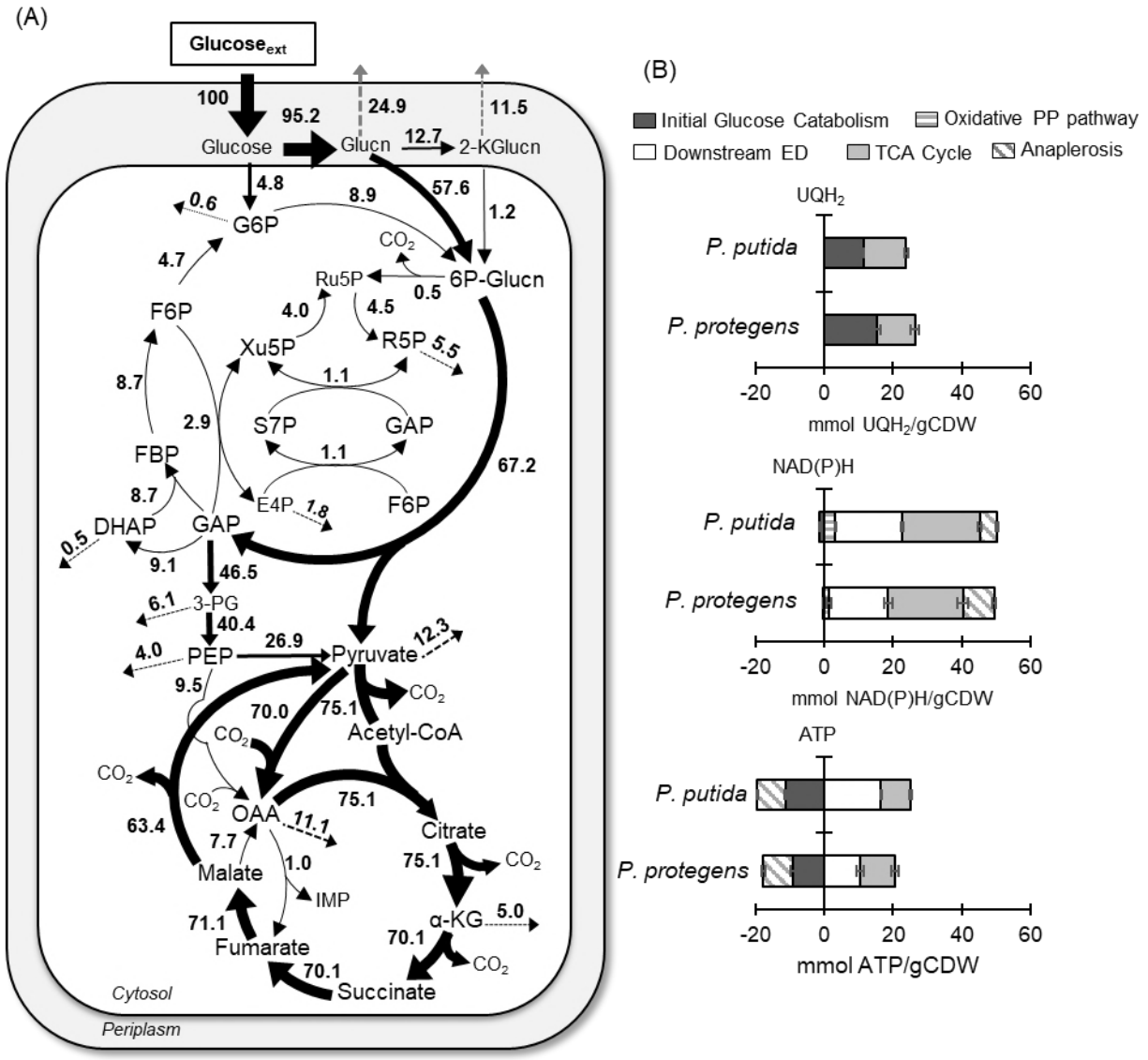

720

721 **FIG 4.** (A) Quantitative metabolic flux analysis and (B) energetic distributions in glucose-grown
722 *P. protegens* Pf-5. All fluxes are normalized to 100% glucose uptake and the thickness of each
723 arrow is scaled to the relative flux percentage. For A, black dotted arrows indicate contribution
724 to biomass and grey dashed arrows indicate excretion fluxes. The absolute fluxes (mean ±
725 standard deviation) are listed in Table S3 and S4. Abbreviations for A are as shown in the legend
726 of Fig. 3. For B, the relative contribution of different pathways to the NAD(P)H, UQH_2, and ATP
727 pools were calculated from metabolic fluxes. Data for *P. putida* KT2440 were obtained from
728 MFA reported in Nikel et al. (10). All values in part B are relative to glucose consumption rate
729 and cellular biomass.

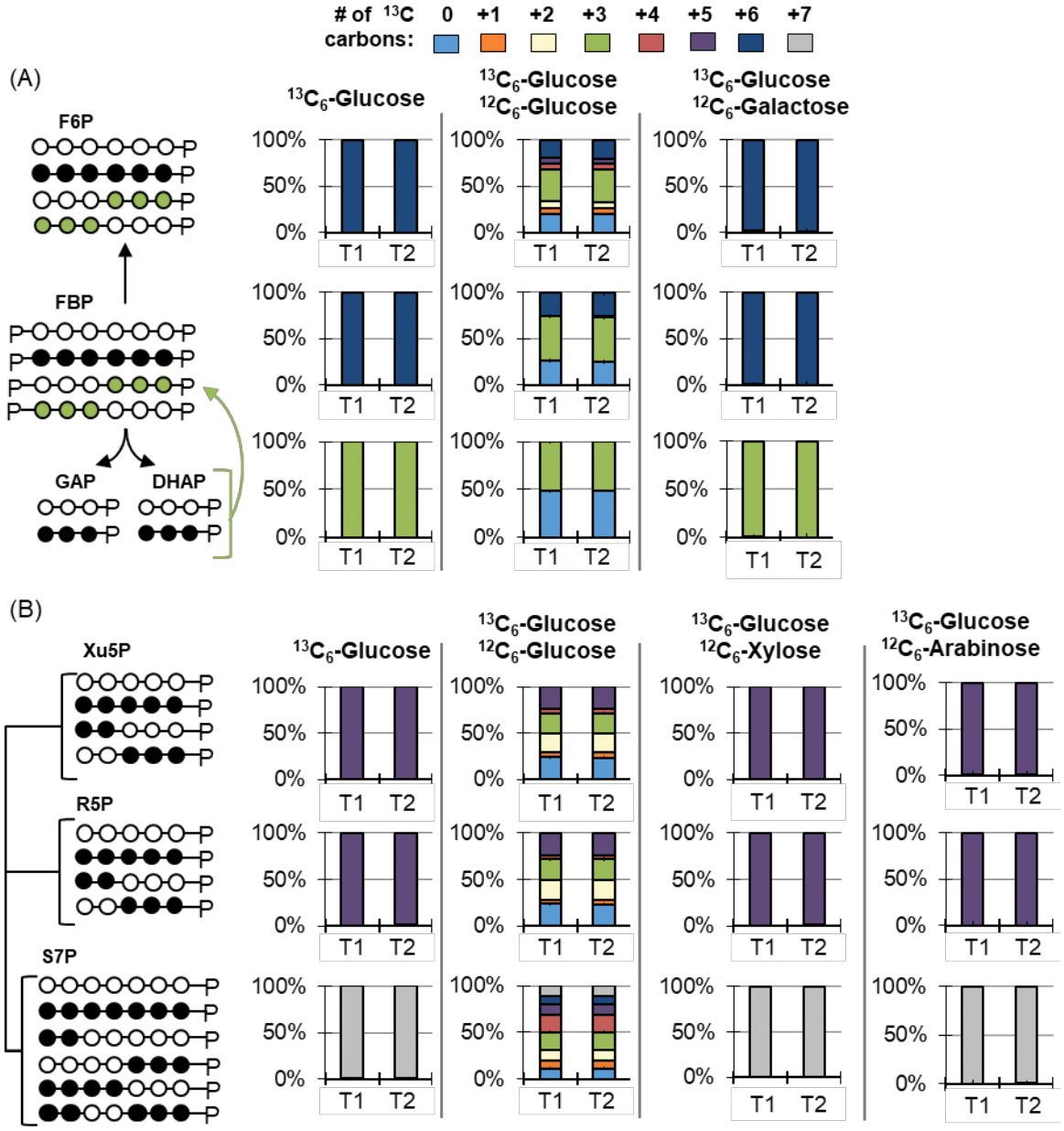

730

731 **FIG 5.** Metabolite labeling patterns during growth on [U-$^{13}C_6$]-glucose ($^{13}C_6$-Glucose) alone or
732 with unlabeled glucose ($^{12}C_6$-Glucose), unlabeled galactose ($^{12}C_6$-Galactose), unlabeled xylose
733 ($^{12}C_6$-Xylose), or unlabeled arabinose ($^{12}C_6$-Arabinose). (A) Carbon mapping (left) and the
734 labeling data (right) for intracellular metabolites in the reverse Emden-Meyerhof-Parnas
735 pathway following feeding on $^{13}C_6$-Gluc alone or with $^{12}C_6$-Gluc or $^{12}C_6$-Gala. (B) Carbon
736 mapping (left) and the labeling data (right) for intracellular metabolites in the pentose-
737 phosphate pathway following feeding on $^{13}C_6$-Gluc alone or with $^{12}C_6$-Gluc, $^{12}C_6$-Xylo, or $^{12}C_6$-
738 Arab. In the carbon mapping, the open circles and the filled circles represent unlabeled and

739 ^{13}C-carbons, respectively. Data were obtained at two timepoints during exponential growth: at
740 OD_{600} 0.5-0.6 (T1) and at OD_{600} 0.9-1.0 (T2). Labeling color legend: nonlabeled carbon (light
741 blue), one ^{13}C-carbon (orange), two ^{13}C-carbons (cream), three ^{13}C-carbons (green), four ^{13}C-
742 carbons (red), five ^{13}C-carbons (purple), six ^{13}C-carbons (dark blue), and seven ^{13}C-carbons
743 (grey). Labeling data (average ± standard deviation) were from three biological replicates. Very
744 small error bars are not noticeable. The abbreviations used for the metabolites are given in Fig.
745 1 and Fig. 3.
746

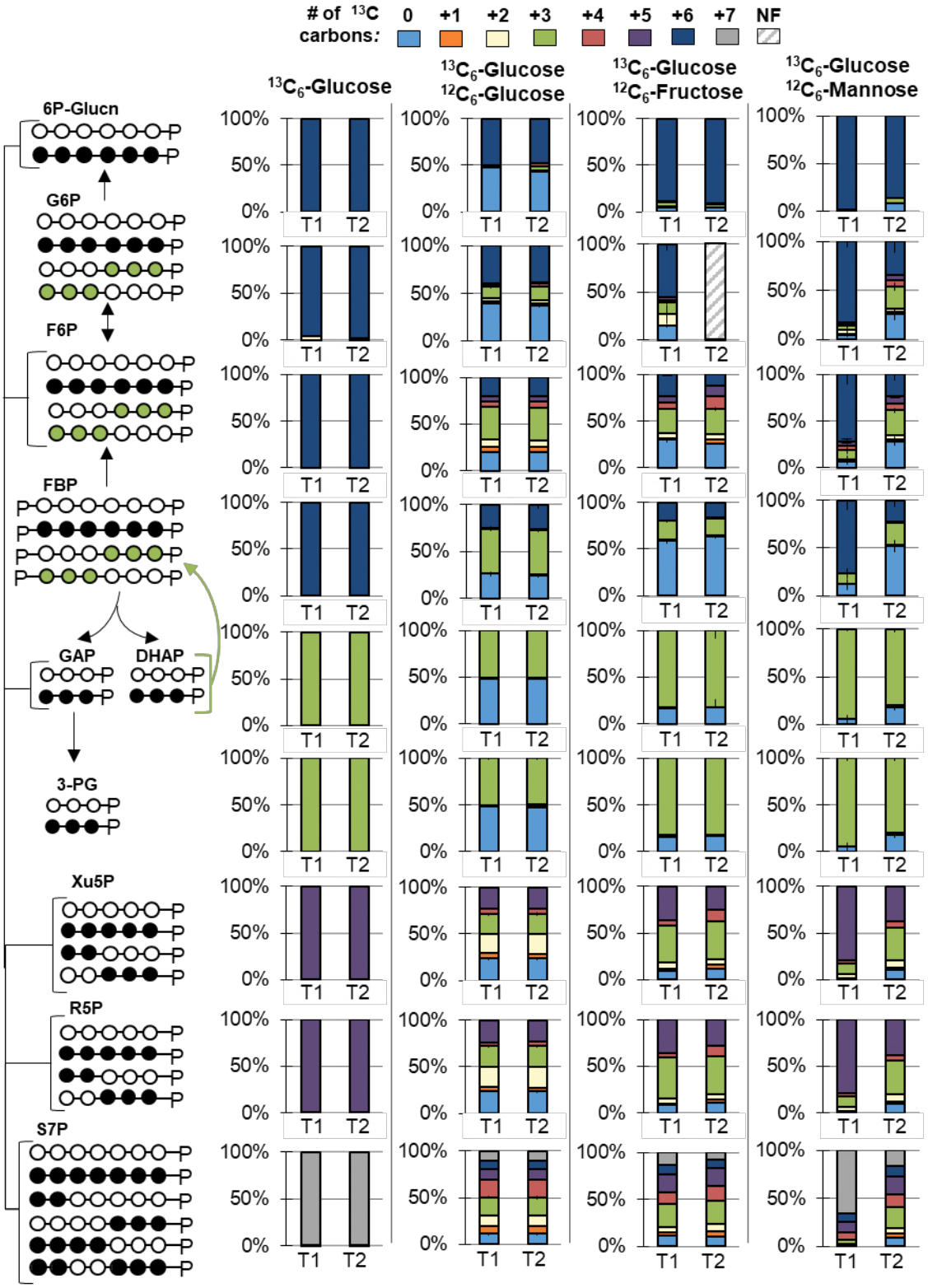

FIG 6. Metabolite labeling patterns during growth on [U-$^{13}C_6$]-glucose ($^{13}C_6$-Glucose) alone or with unlabeled glucose ($^{12}C_6$-Glucose), unlabeled fructose ($^{12}C_6$-Fructose), or unlabeled

mannose ($^{12}C_6$-Mannose). Carbon mapping (left) and the labeling data (right) for intracellular metabolites in the Entner-Doudoroff pathway, reverse Emden-Meyerhof-Parnas (EMP) pathway, and the pentose-phosphate pathway. The open circles and the filled circles represent unlabeled and ^{13}C-carbons, respectively; the-green colored circles represent labeling schemes specifically from reverse flux through upper EMP pathway. Data were obtained at two timepoints during exponential growth: at OD_{600} of 0.5-0.6 (T1) and at OD_{600} of 0.9-1.0 (T2). Labeling color legend: nonlabeled carbon (light blue), one ^{13}C-carbon (orange), two ^{13}C-carbons (cream), three ^{13}C-carbons (green), four ^{13}C-carbons (red), five ^{13}C-carbons (purple), six ^{13}C-carbons (dark blue), and seven ^{13}C-carbons (grey). NF, not found. Labeling data (average ± standard deviation) were from biological replicates (*n* = 3). Very small error bars are not noticeable. The abbreviations used are given in the legend of Fig. 1 and Fig. 3.

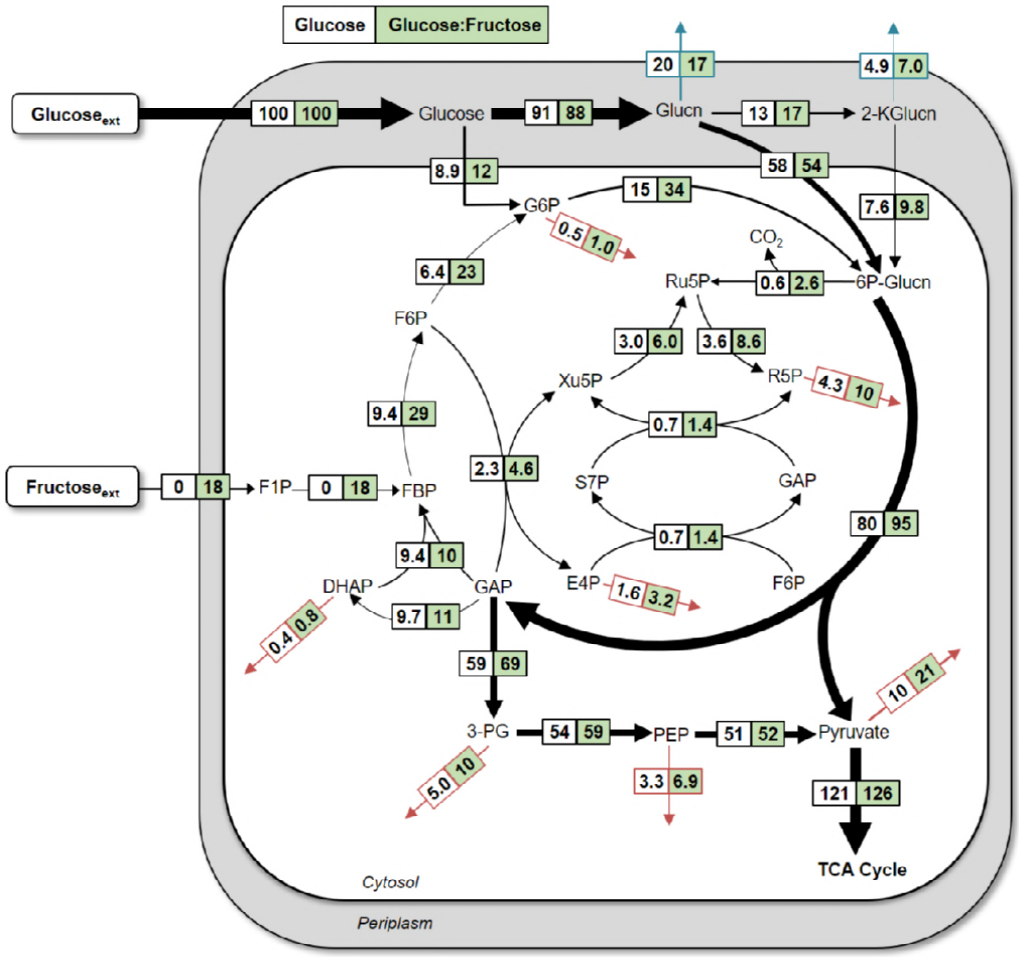

761

762 **FIG 7.** Quantitative metabolic flux analysis of *P. protegens* Pf-5 using metabolite labeling data
763 following growth on [U-$^{13}C_6$]-glucose:unlabeled glucose (white) or [U-$^{13}C_6$]-glucose:unlabeled
764 fructose (green). All fluxes were normalized to 100% glucose uptake and the thickness of each
765 arrow was scaled to the relative flux percentage for the glucose-only growth condition. The
766 absolute fluxes (mean ± standard deviation) are listed in Table S5 and S7. Red arrows indicate
767 contribution to biomass and blue arrows indicate excretion fluxes. The metabolite
768 abbreviations are as given in the legends of Fig. 1 and Fig. 3.

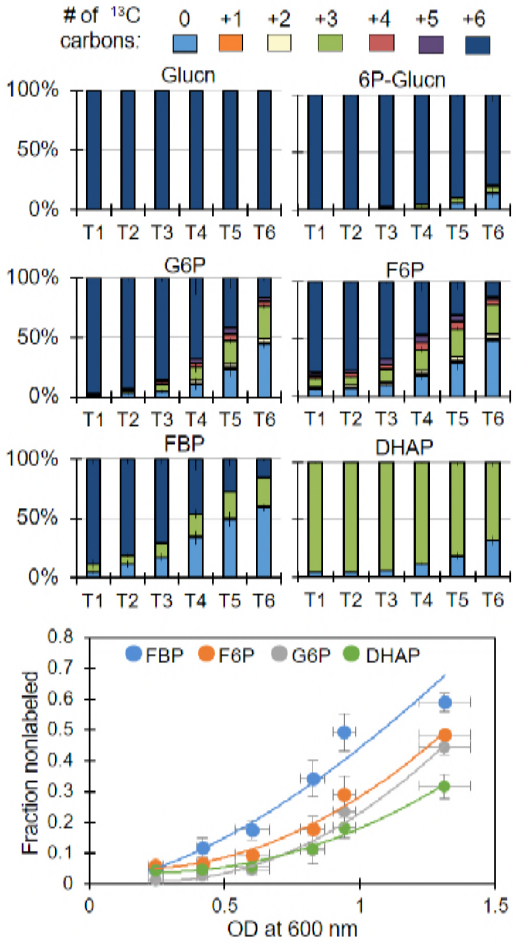

769

770 **FIG 8.** Kinetic profiling of metabolite labeling patterns in cells grown on [U-$^{13}C_6$]-glucose and
771 unlabeled mannose. Labeling color legend: nonlabeled carbon (light blue), one ^{13}C-carbon
772 (orange), two ^{13}C-carbons (cream), three ^{13}C-carbons (green), four ^{13}C-carbons (red), five ^{13}C-
773 carbons (purple), six ^{13}C-carbons (dark blue). Data were obtained at six timepoints during
774 exponential growth: at OD_{600} of 0.21-0.27 (T1), at OD_{600} of 0.40-.44 (T2), at OD_{600} of 0.54-0.67
775 (T3), at OD_{600} of 0.79-.87 (T4), at OD_{600} of 0.90-0.98 (T5), and at OD_{600} of 1.2-1.4 (T6). The data
776 (average ± standard deviation) are from biological replicates (*n* = 3). The lines through the data
777 in the bottom figure represent guide to the eye. The metabolite abbreviations are as given in
778 the legends of Fig. 1.